Self-adaptive and self-healing nanocomposite tribocoatings

Cao, Huatang

CHAPTER 3

Effect of carbon concentration and argon flow rate on the microstructure and tribological properties of magnetron sputtered WS_2/a-C coatings*

In this chapter, WS_2/a-C coatings with various carbon contents (0-65 at.%) were deposited on single crystal silicon wafers by magnetron co-sputtering under different Ar flow rates. Increasing the argon flow rate increases the chemical stoichiometric S/W ratio, but the coating gradually becomes porous and columnar-like. The S/W stoichiometry is less influenced by the variations in carbon concentration. TEM and XRD confirm well crystallized basal (002) planes in the pure WS_x or low-carbon WS_2/a-C films. The hardness of the composite coatings increases with increasing carbon content or decreasing flow rate from 25 sccm to 10 sccm Ar. The coating at 40 at.% C exhibits the highest hardness (10.6 GPa). Tribotests show that the coefficient of friction can be low 0.02 in dry air (5% R_H) and around 0.15 in moisture (55% R_H) and remains stable within the first 1000 meters with a low wear rate of 10^{-7} $mm^3/m^{-1}N^{-1}$. The wear resistance is strongly affected by the carbon concentration, deposition pressure and the testing atmospheres.

* This chapter has been published in the following journal:
H.T. Cao, J.Th.M. De Hosson, Y.T. Pei. ***Surf. Coat. Technol.*** 332(2017) 142-152.
DOI: http://dx.doi.org/10.1016/j.surfcoat.2017.06.087

3.1 INTRODUCTION

Layered transition metal dichalcogenides (TMD) have a structure of an X–Me–X type (MeX_2, Me = W, Mo; X = S, Se) with a strong anisotropy in their mechanical and electrical properties, making it the focal point of intensive research studies. In this class of materials, WS_2 is a material well-known for their solid lubrication properties. WS_2 crystallizes in the hexagonal anisotropic structure, in which a layer of tungsten atoms is sandwiched between two hexagonally packed layers. The bonding within the layer is covalent, whereas the bonding between the adjacent layer consists of weak Van der Waals interactions, resulting in easy planar glide and low friction [1, 2]. In addition, such crystals can be readily sheared to generate clean and almost atomically smooth surfaces under sliding [3]. Sputtered WS_2 coating has been widely used in transport, e.g. aerospace applications due to its ultra-low friction coefficient (CoF) in the high vacuum environment [4, 5]. However, similar to MoS_2, WS_2 lubricants are soft, not abrasion resistant, and easily degrade in air and humid environment. To comply with endurance requirements of aerospace applications, other advanced approaches are being explored. One of them is self-lubricating composites, where solid lubricant is pressed into an amorphous diamond-like carbon (DLC) supporting matrix. DLC films are reported to have many features that contribute to excellent tribological characteristics, such as high hardness, anti-wear property with both low friction coefficient and low wear rate (W_R) against many different counterface materials [6, 7]. The compliant amorphous carbon matrix may generate a high density of interphase interfaces that assist in crack deflection, termination of columnar growth and protection WS_2 from oxidation [8, 9].

Although previous research has reported breakthroughs in fabricating WS_2/a-C composite lubricant coatings with a low friction coefficient (< 0.05) in dry environment, the tribological properties of WS_2/a-C based coatings are strongly influenced by the chemical composition and deposition parameters [9]. It is known that sputtered TMD films are usually not stoichiometric, i.e. MeX_{2-y}, where Me is Mo or W, and X is S or Se with $y > 0$ [5, 9-14]. Since lubrication properties of the films rely strongly on the stoichiometry, a very precise control of the sputtering parameters is indispensable if TMD layers are to be prepared in a reproducible way with high quality. As reported by Cavaleiro et al. [13, 15], the S/W ratio increased with carbon addition, but the Se/W ratio of co-sputtered WSeC coatings was recorded between 0.9 and 1.0, showing no significant influence of the carbon content on their variations [16]. The substoichiometry is generally attributed to the preferential resputtering of sulfur due to the bombardment of neutral argons reflected on the targets [17-19] and the reactions between MeX_2 and residual atmosphere [9].

The sulfur stoichiometry also influences the crystallography and tribological behaviors of MeSC coating. As the sulfur content increases, the (002) lamellar crystallites become more pronounced and the size of grains increases in the form of dendritic-like branches [5, 22-24]. Voevodin [5] found in WS_xC coatings when $x = 0$ WC nanoclusters surrounded by amorphous DLC. Beyond a sulfur concentration of $x = 29$ at.% the coating demonstrated the presence of hexagonal WS_2. Even more interesting is that the composite with sulfur content below 15 at.% had a surprisingly high friction coefficient of 0.5-0.7 in vacuum and 0.2-0.3 in dry nitrogen, in agreement with the single-phase unhydrogenated DLC in vacuum. The amorphous carbon with partial graphitization as confirmed by Raman tests on the wear tracks suggest that DLC plays the predominant role in dry sliding when sulfur is depleted.

One should keep in mind that the literature indicates (see [14, 22, 25]) that the coating deposition parameters such as argon pressure can strongly influence the microstructure and mechanical properties of the TMD tribocoatings. The present work concentrates on the synergetic effects of carbon content and argon flow rate on the microstructure, composition, morphology, mechanical behavior and tribological performance, which were scantly reported in detail before. In particular the following points will be addressed:

- What is the influence of carbon content and argon flow rate on the microstructure and composition of the nanocomposite coatings?
- Can the relatively soft sputtered pure WS_2 films also have a long wear life?
- What is the role played by S/W stoichiometry on tribological properties and will a WS_2 film with a higher crystallinity necessarily leads to a superior wear performance?

3.2 Experimental procedures

3. 2.1 Preparation of the WS_2/a-C coatings

The W-S-C coatings were deposited on single crystal silicon wafers (100). The substrates were first ultrasonically cleaned in acetone followed by Ar plasma etching for 20 min at p-DC - 400 V bias voltage at 250 kHz and 87.5% duty cycle. Finally, two WS_2 targets (p-DC mode) and one graphite target (DC mode) were sputtered in a pure Ar atmosphere to deposit the films. Power supply (Advanced Energy) and the other magnetron coupled to Cr target were powered by a Pinnacle 6/6 kW double channel DC power, which was employed to produce a Cr interlayer having a thickness approximately 300 nm to increase the interfacial adhesion. It should be noted that all the power units for sputtering were operated in a current-control mode. The current

applied to the two WS_2 targets was set at both 0.5A corresponding to a voltage of ~ 530 V at 150 kHz pulse frequency (70 % duty cycle) while the current applied to one C graphite target and the number of WS_2 targets (99.9% purity) used was altered to change the carbon content in the nanocomposite coating. The coating deposition process time was 2h for all samples. The substrates were self-biased using a floating potential. The base pressure of the chamber before deposition was $3\text{-}5\times10^{-4}$ Pa. The substrates were mounted vertically to the surface of a carousel that rotates 3 rpm in front of the targets with no external heating. In order to study the microstructure, composition, morphology and deposition rate as a function of argon flow rate, the films were deposited at 10, 15, 20 and 25 standard cubic center meter per min (sccm). 10 sccm Ar flow rate corresponds to an Ar pressure of around 0.3 Pa. The deposition rate was roughly calculated by dividing the cross-section thickness of the coating by the deposition time.

3.2.2 Characterization of the WS_2/a-C coatings

The microstructure was investigated using an environmental scanning electron microscope (ESEM, FEI FEG-XL30), high resolution transmission electron microscope (HR-TEM, 2010F-JEOL). Atomic force microscope (AFM, Digital Instruments NanoScope 3100) was used to characterize the surface morphology. Energy dispersive spectrum (EDS) with an accelerating voltage of 20 kV in FEI XL30 SEM were employed to determine the chemical composition of the films. The EDS are tested on three random areas of each sample. Standard theta/two theta spectrum of the WS_2 powder was measured by Bruker D8 diffractometer while the grazing incidence X-ray diffraction (GI-XRD) spectra were measured by PANalytical-X'Pert MRD to probe the top surface phases using a 2.5° incident angle in parallel beam geometry. MTS Nano indenter XP® equipped with a Berkovich indenter was employed to measure the hardness (H) and elastic modulus (E) of the films. The maximum indentation depth for measuring H and E was approximately 200 nm, corresponding to less than 10% of the film thickness. Raman spectra with a He–Ne laser (632.8 nm) at approximately 1-2 mW at a wavelength range of 200–2000 cm^{-1} were obtained to investigate the phases in the wear tracks. Raman probing area and depth are around 10 μm^2 and 250 nm, respectively. The tribological properties of these films were investigated using a CSM tribometer with a ball-on-disk configuration, against Φ6 mm 100Cr6 steel balls at a fixed sliding speed of 10 cm/s for 1000 m at room temperature (20–23 °C). All tribotests were conducted in both dry air (relatively humidity of 5%, radius 7.5 mm corresponding to ~ 21000 revolutions) and under high humidity (relatively humidity of 55 %, radius 9 mm corresponding to ~ 18000 revolutions) respectively, tailored by a home-made humidity modulator. The hardness value of the steel balls is 7.5 GPa, giving an initial mean Hertz contact pressure of ~ 0.7 GPa with 5N normal load. After

wear tests, wear scars were characterized by SEM. 3D confocal micrographs (705×725 μm^2) of the wear tracks on the coatings were captured to measure the removed wear volume for the calculation of wear rates of the films under different deposition and tribological conditions. Normalized wear rates ($mm^3\ N^{-1}\ m^{-1}$) were estimated through a Matlab code according to the following equation: $K = V/(L \times s)$, where V being the wear volume, s the total running distance of the ball over the disk, and L the normal applied load.

3.3 Results and Discussions

3.3.1 Basic characteristics of WS_2

Figure 3.1 shows the microstructure of the powders directly scratched from the WS_2 target. **Figure** 3.1a shows a SEM image of obviously lamellar microstructure of WS_2 powders. In general, sputtered MeX_2 has two types of orientations: type I films with structurally well-developed lamella vertical to the coating substrate (edge orientation: c ||), complemented by dendritic branches that are sensitive to oxygen leading to poor wear; type II films with microcrystallized layers parallel to the substrate (basal orientation: c ⊥) that are inert to environmental attacks and could afford superior lubrication [22]. Crystal structure of hexagonal 2H-WS_2 with easy shear plane (002) are apparently evidenced in the WS_2 target material as indicated in **Figure** 3.1b. Furthermore, the θ-2θ XRD spectrum (see **Figure** 3.1c) indicates the strongest and well crystallized basal orientation peaks of (002) and some other typical peaks showing the edge orientations such as (101) at angle of ~ 34 ° and (110) at angle of ~ 58° respectively (JCPDS No. 008-0237).

3.3.2. Chemical and structural characterization

Table 1 shows that the chemical composition of sputtered WS_2/a-C coatings changes upon the sputtering current of graphite target and argon flow rate from 10 sccm to 25 sccm. A fixed current of 0.5 A (Coating No.1-12) and 0.3 A (Coating No. 13-14) was applied to each WS_2 target. For coatings No. 11-14, the use of only one WS_2 target aims at tailoring the carbon content to a maximum of around 65 at.%. As can be seen, around 1-3 at.% oxygen is embedded in all the sputtered coatings due to residual oxygen in the PVD chamber. The carbon concentration increases with increasing current applied to one graphite target from 0.5 A to 1.5 A and the reduction of two WS_2 targets to one. For instance, carbon in these coatings increases from ~ 21 at.% (0.5 A applied on graphite target) to ~ 40 at.% (1.5 A applied on the graphite target). While the graphite target keeps at 1.5 A, the use of one WS_2 target with reduced current from 0.5 to 0.3 A could further increase the carbon content to ~ 65 at.%. In contrast, the content of both sulfur and tungsten shows a decreasing trend with increasing carbon. The content of

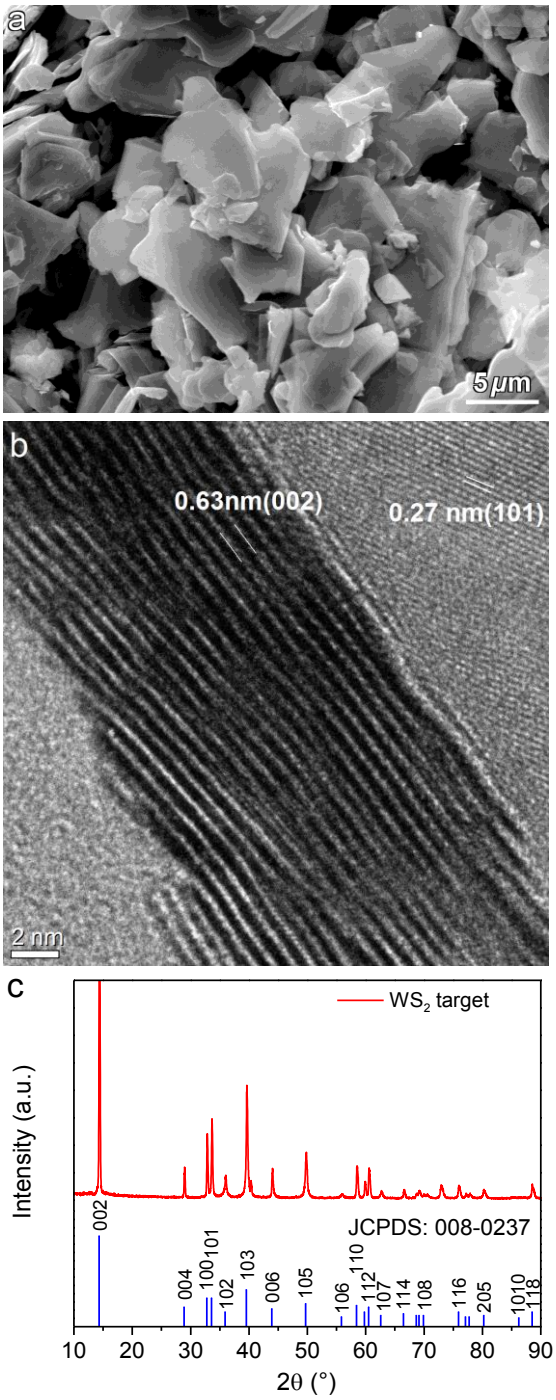

***Figure** 3.1 As-received WS_2 target: (a) SEM and (b) TEM images showing lamellar structure and (c) XRD spectrum.*

Table 3.1 Composition of WS_2/a-C under different deposition conditions (ESEM, 20 kV).

Sample No.	Deposition condition			Deposition rate (nm/min)	Composition (at.%)				S/W ratio
	WS_2* (A)	Graphite (A)	Ar flow (sccm)		C	O	S	W	
1	0.5	-	10	13.1	-	2.3 ± 0.2	59.5 ± 0.3	38.2 ± 0.3	1.56
2	0.5	-	25	30.3	-	2.9 ± 0.2	61.9 ± 0.3	35.2 ± 0.1	1.76
3	0.5	0.5	10	12.3	21.8 ± 0.5	2.0 ± 0.1	43.9 ± 0.4	32.3 ± 0.1	1.36
4	0.5	0.5	15	14.1	17.2 ± 1.6	2.0 ± 0.2	49.0 ± 1.0	31.8 ± 0.7	1.54
5	0.5	0.5	20	15.3	19.1 ± 0.7	2.1 ± 0.4	49.2 ± 0.5	29.6 ± 0.2	1.66
6	0.5	0.5	25	16.3	16.9 ± 0.2	2.1 ± 0.1	51.6 ± 0.2	29.4 ± 0.2	1.76
7	0.5	1.5	10	14.8	39.6 ± 0.5	1.3 ± 0.1	33.7 ± 0.4	25.4 ± 0.2	1.33
8	0.5	1.5	15	16.8	35.3 ± 1.1	2.0 ± 0.3	36.9 ± 0.6	25.8 ± 0.6	1.43
9	0.5	1.5	20	17.6	34.5 ± 1.4	2.3 ± 0.2	38.8 ± 0.9	24.4 ± 0.6	1.59
10	0.5	1.5	25	19.3	33.2 ± 1.1	2.1 ± 0.3	41.2 ± 0.8	23.6 ± 0.5	1.75
11	0.5(×1)	1.5	10	10.2	51.3 ± 0.1	1.2 ± 0.1	27.3 ± 0.3	20.2 ± 0.1	1.35
12	0.5(×1)	1.5	25	12.3	46.6 ± 0.4	2.1 ± 0.1	32.3 ± 0.3	19.0 ± 0.2	1.70
13	0.3(×1)	1.5	10	7.3	64.2 ± 1.0	1.3 ± 0.1	19.9 ± 0.6	14.6 ± 0.5	1.36
14	0.3(×1)	1.5	25	9.0	61.3 ± 0.4	1.9 ± 0.4	23.6 ± 0.5	13.2 ± 0.1	1.79

* Two WS_2 targets were used for deposition, unless otherwise stated one WS_2 target by (×1).

sulfur maximizes at ~ 62 at.% when no carbon is added under 25 sccm Ar and reaches a minimum of ~ 20 at.% when a lowest current (0.3 A) is applied to the WS_2 target under 10 sccm Ar.

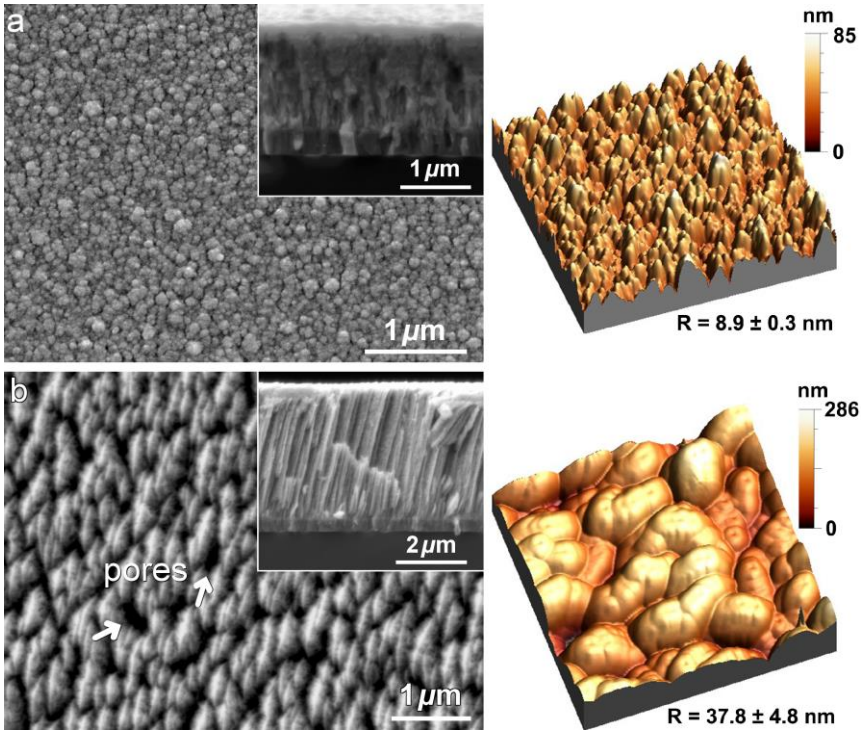

***Figure** 3.2 SEM micrograph (left) and AFM micrograph (2×2 μm²) showing the effect of Ar flow rate on the microstructure and surface morphology of pure WS_2 films deposited at (a) 10 sccm Ar and (b) 25 sccm Ar (Note: R refers to root mean square roughness).*

Ar flow rate, which directly correlates with the working pressure, strongly influences the coating chemical compositions. As shown in Table 1, the comparison between coating group No. 3-6 and group No. 7-10 manifests that a gradual increase in sulfur coincides with a decrease in tungsten as Ar flow rate rises from 10 sccm to 25 sccm. A slight variation in carbon concentration is also observed. More interesting is to note in Table 1 that the stoichiometric ratio of sulfur to tungsten (S/W), being more or less independent of carbon fluctuations, increases from ~ 1.31 to 1.76 as a function of growing Ar flow rate. Sarhmmar et al. [26] combined Monte Carlo simulations and experiments to investigate the compositional variations of sputtered WS_2 and also concluded that S/W ratio is only slightly influenced by the target voltage (equal to the target current here), while the most significant variations are attributed to the processing pressure and positions on the chamber. At lower pressure, substantial

sulfur resputtering take places due to both rising plasma potential and decreasing thermalization, triggering irradiation of the growing film by energetic particles from the plasma (Ar^+) and also from the target, e.g. W, S or probably backscattered neutral Ar [26, 27]. Therefore, lowest sulfur content ($WS_{1.31}$) are found in films deposited at 10 sccm Ar. In the case of a higher argon pressure (25 sccm) and hence a short mean free path (λ_{mpf} positively correlates with P^{-1}) causing higher frequency of species scattering and collisions, the energetic particles, i.e. particularly the large and heavy Ar atoms will greatly lose the energy before reaching the substrate surface and sulfur resputtering will be reduced because of the alleviated impingements [11, 28].

In addition, Ar pressure also affects the surface topography to a large extent. Under 10 sccm Ar flow, **Figure** 3.2a shows the pure WS_2 coating resembles a typical cauliflower-like PVD sputtered DLC coating with a rough surface (Rq = 8.69 nm). On the other hand, the pure WS_2 films sputtered at 25 sccm Ar (see **Figure** 3.2b) exhibits obviously a flaky and porous microstructure with an exceedingly high Rq = 42.10 nm, structurally similar to the sputtered porous pure MoS_2 films reported in [29, 30]. The inset cross-section images of **Figure** 3.2 show that pure WS_2 thin films presents columnar plate zone II morphology (Thornton model ref [31]) with typical inherent porosities [31], corresponding to extremely low hardness and high wear rate that are discussed later. Large voids clearly appear in WS_2 under 25 sccm Ar in **Figure** 3.2b.

When it comes to WS_2/a-C coating as shown in **Figure** 3.3, the domed-like coatings evidently exhibit densified morphologies than pure WS_2. For instance, **Figure** 3.3a-d shows the morphologies of the coatings, deposited at 0.5 A applied to the graphite target yielding to ~ 20 at.% C, vary as a function of Ar flow rate. It can be seen that more porosities are observed with increasing Ar flow rate from 10 sccm (**Figure** 3. 3a) to 25 sccm (**Figure** 3.3d). Particularly the one under 25 sccm Ar presents typical dendritic growth with columnar structure, even close to the pure WS_2 film under 10 sccm Ar indicated in **Figure** 3.2b. AFM images displayed in **Figures** 3.3i-j confirm that the increasing pressure goes together with a marked coarsening of the morphology, as characterized by an increasing roughness. However, compared with pure WS_2, it should be pointed out that the RMS drops from 8.69 nm to a minimum of 3.65 nm (both 10 sccm Ar), indicating the formation of a denser coating with ever flatter top morphologies due to the contribution of carbon additions. When the carbon content rises to the range of ~ 40 at.%, further compact coatings are formed as shown in **Figures** 3.3e-h. The inset of **Figure** 3.3e indicates WS_2/a-C coating deposited at low Ar pressure turns out column-free and featureless, corresponding to zone I morphology. This is because the intense ion impingement under low pressure condition and carbon additions significantly densify the microstructure.

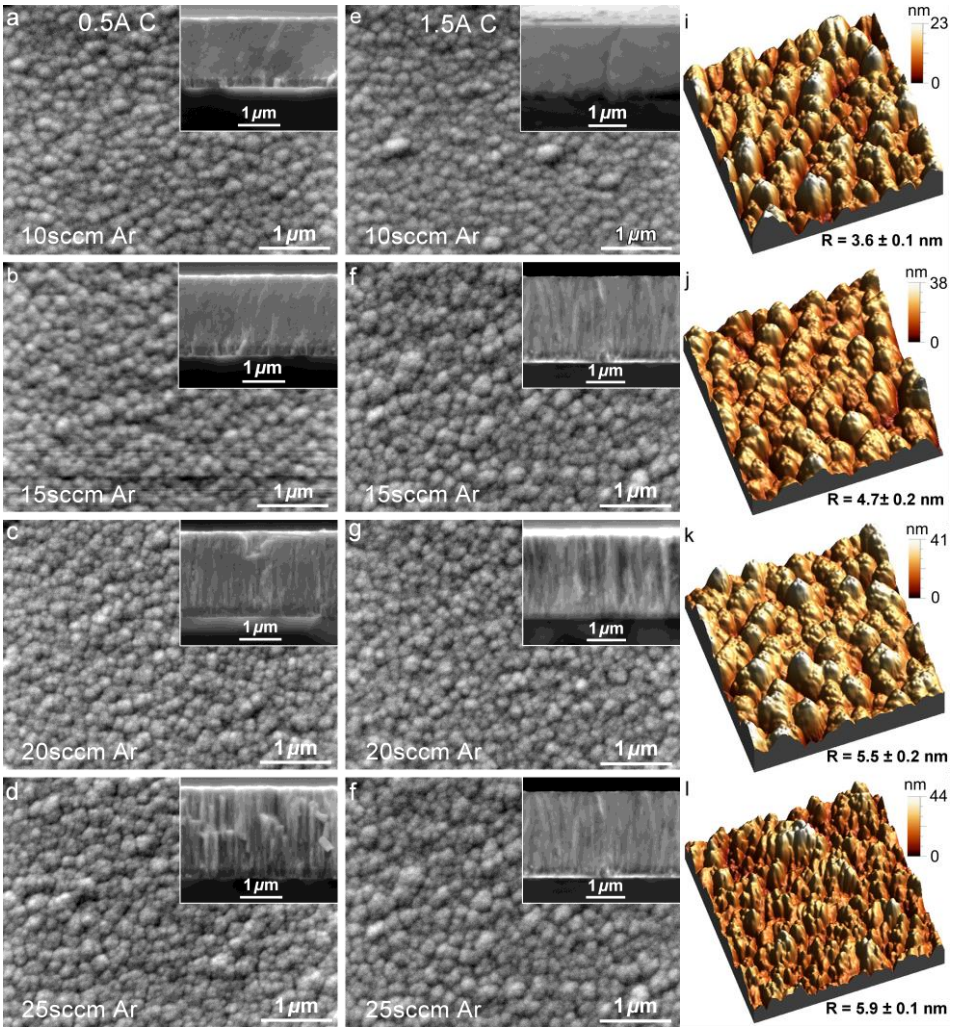

***Figure** 3.3 Effect of carbon and Ar flow rate on the surface morphology and microstructure of WS_2/a-C coatings: (a-d) 0.5A C with Ar flow rate indicated; (e-h) 1.5A C with Ar flow rate indicated; (i-l) AFM surface topography (2×2 μm^2) of WS_2/a-C coatings of (a-d) respectively.*

It is worth mentioning that the deposition rate also increases with increasing Ar flow rate as listed in Table 1. Possible reasons are that higher gas pressure results in higher ion density and thus more amount of materials are sputtered away from the targets [32]. Also the sputtering yield is enhanced due to increased probability of an ion colliding with gas atoms during its traverse across the cathode dark space, which promotes the percentage of ions striking the target at oblique angles of incidence [32]. The pure WS_2 film under 25 sccm Ar features with the highest deposition rate reaching

a striking high value of ~ 30 nm/min. This is, however, partially because of the lowest density due to such WS_2 film with porous structure [17].

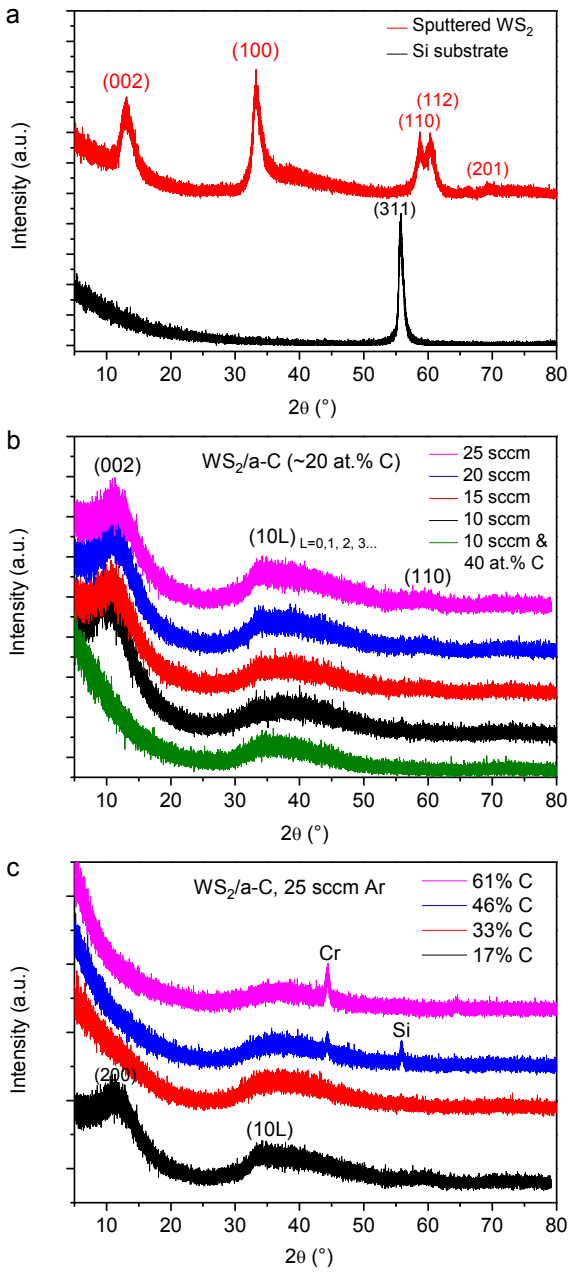

***Figure** 3.4 Grazing incidence X-ray diffraction spectra: (a) sputtered pure WS_2 and Si substrate; (b) as a function of Ar flow rate (~ 20 at.% C unless stated); (c) as a function of carbon content (Cr peak emerges from the Cr interlayer due to thinner coatings [30]).*

The diffraction patterns for sputtered WS_2 and WS_2/a-C films as a function of Ar flow rate and carbon content are shown in **Figure** 3.4. **Figure** 3.4a shows the typical hexagonal WS_2 peaks (002) at $2\theta = \sim 14°$, fitting in well with WS_2 powders as indicated in **Figure** 3.1c. Such strong intensity (002) reflection indicates that numerous WS_2 crystals are oriented with basal planes parallel to the surface, which is typical type Ⅱ structure for sputtered TMD coatings.

TEM image of **Figure** 3.5a further confirms that the lamellae extend more than 20 nm in length (with $c \perp$) and are exclusively parallel with silicon substrate. However, consistent with Ref. [22, 33], such wider (~ 0.6 nm) spaced (002) basal planes only grow for tens of nanometers along substrate and then (002) planes turn random or even perpendicular to the substrate (see **Figure** 3.5a). Even narrower (0.3 nm) edge planes such as (101), (103) starts to form (see **Figure** 3.5b). Moser et al.[33] suggested that the transition from the parallel layer to the perpendicular crystallites occurs via a branching process during growth as the crystallites seems to be preferentially oriented vertical to one another. **Figure** 3.4b shows that the diffraction patterns become less distinct with increasing carbon. From 10 sccm to 25 sccm, a slight increase in crystallinity could be observed, and under 25 sccm and 20 sccm Ar the (110) peak is also visible. **Figure** 3.4b also indicates that an asymmetrical (100) peak around $2\theta = 33°$ with a long tail. This is commonly attributed to the effect of the turbostratic stacking of WS_2 basal planes. It is known that in the hexagonal lattice structure the (00l) reflections correspond to the ordering in the c-direction while the (hk0) reflections to the basal planes. Weise et al. [14] suggested that the referred XRD patterns of TMD points to a two-dimensional (2D) organization of the basal plans which could have several tenths of unit cells. The stacking of the a-b basal lattice planes in the c-direction, provided lateral dimensions within the range of a few nanometers, leads to a sharp peak at approximately the position for the (100) reflections. It tails towards larger angles suggesting other reflections of the (10L) family with L =1, 2 3…[14, 27, 34-36] and presenting a broad peak typical of an amorphous structure. Another slightly asymmetric peak is observed at the position for the (110) reflections at $2\theta = \sim 58°$. As stated earlier, WS_2/a-C films brings out enhanced structural densification and the diffraction pattern starts to exhibit broader peaks, indicating smaller or shorter crystallites than that in pure WS_x films. It is worth mentioning that the most important diffraction pattern of (002) basal plane, in fact absent in the reported XRD spectra of earlier TMDs [9, 34, 35], remains visible over the entire range of argon flow rates from 10 to 25 sccm in the coatings No. 3-6. This could be further validated by **Figure** 3.4c, where the (002) basal planes start to disappear when the carbon content surpasses 33 at.%. Furthermore, the (10L) turbostratic stacking planes also become even broader when the carbon concentration goes up to 46 at.%. It indicates that coatings with high carbon content lose crystallinity and gradually

turning out x-ray amorphous. Some Si peaks from the substrate (refer to **Figure** 3.4a) and Cr peaks from the interlayer arise due to the decreased thickness (only 0.3 A applied to one WS_2 target) of the high-carbon coatings illustrated in Table 1. Furthermore, comparison of **Figure** 3.4b with pure WS_2 film in **Figure** 3.4a shows that a slight shift for (002) towards lower diffraction angles occurs after WS_2 doping with carbon, implying an increased lattice parameters of WS_2 after carbon addition [34]. HR-TEM images of **Figure** 3.5c show that the nanocrystalline WS_2 phases, with a platelet shape, are randomly oriented in an amorphous carbon matrix, see also [5, 23, 24, 37, 38]. TEM micrographs of **Figure** 3.5d and f show short-range ordering of WS_x with Ar flow rate reduced from 25 to 10 sccm. From the high carbon WS_2/a-C film (**Figure** 3.5d, S/W = 1.31), the tiny WS_2 platelets are almost completely surrounded by the C-matrix. The circled darkened areas in **Figure** 3.5d indicate possible formation of some WC nanoclusters similar as reported in [5, 23], although no distinct peaks of WC carbides are visible from each XRD spectrum. TEM images also confirm the loss of WS_2 crystallinity with a lower Ar flow rate, which correlates with decreasing sulfur content because of strong resputtering of sulphur occurring in low pressure deposition [22].

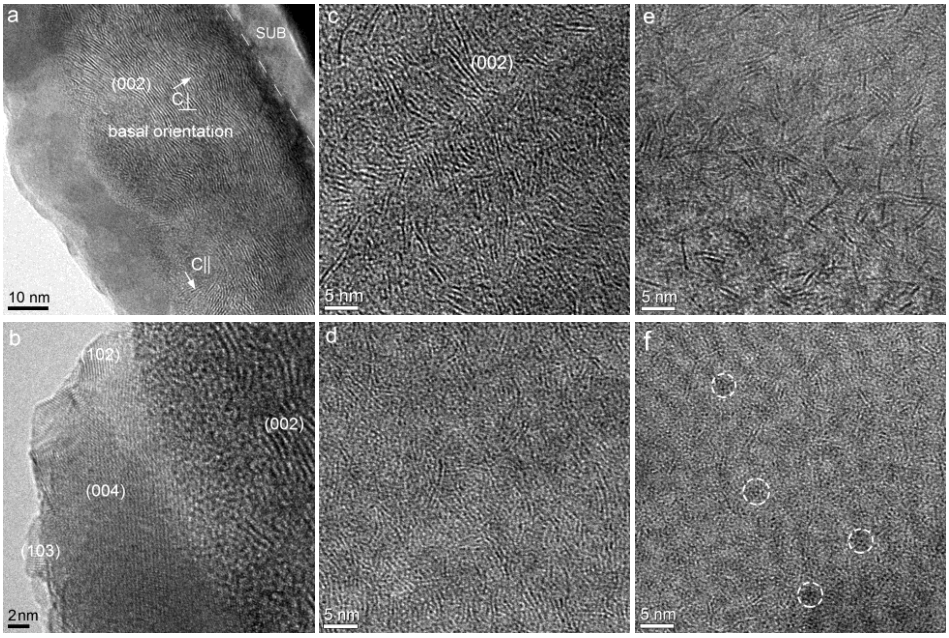

***Figure** 3.5 HR-TEM images of sputtered pure WS_2 film: (a) first tens of nanometers growth of (002) basal orientation along the substrate, (b) further growth of edge orientations; and WS_2/a-C films under different deposition conditions: (c) 0.5A C, 25 sccm Ar; (d) 0.5A C, 10 sccm Ar; (e) 1.5A C, 25 sccm Ar; (f) 1.5A C, 10 sccm Ar.*

3.3.3 Mechanical and tribological properties

Figure 3.6 shows the average hardness and elastic modulus of the coatings measured by depth-sensing nanoindentation using a Berkovich tip. The pure WS_2 film, particularly under 25 sccm, proves to have an extremely low hardness (0.31 GPa) and elastic modulus (12.68 GPa), which is reasonable considering its high porosity and columnar structure (see **Figure** 3.2b). This is close to earlier reported values of TMD hardness (< 0.5 GPa) [17, 20]. However, an increase in hardness of more than one order of magnitude could be achieved whenever WS_2 film is alloyed with C or with a decreasing Ar flow from 25 sccm to 10 sccm. **Figure** 3.6a indicates that a lower Ar pressure promotes the hardness enhancement among the coatings with almost same content of carbon. 10 sccm Ar deposition pressure yields to a hardness of 8.66 GPa in comparison to reduced 5.43 GPa in 25 sccm. Elastic modulus variations accompany the trend of hardness variations closely (see **Figure** 3.6b). Also it is important to note that WS_2/a-C coatings, apart from significantly harder than pure WS_x films, are becoming

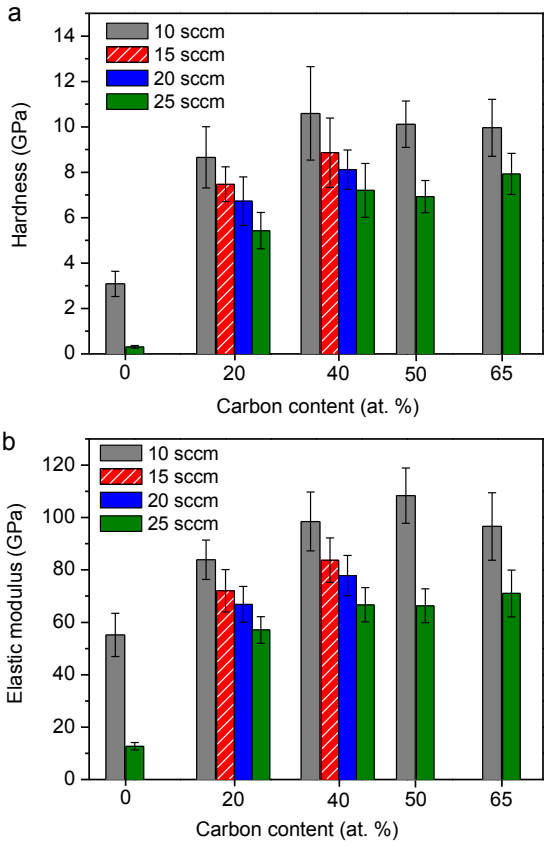

***Figure** 3.6 (a) hardness and (b) elastic modulus of WS_2 and WS_2/a-C coatings deposited at different argon flow rates and of different carbon contents measured by nanoindentation.*

harder with an increasing carbon content until ~ 40 at.%, at which the coating reaches a maximum hardness value of 10.60 GPa, comparable to previous results [15, 21, 34, 37]. WS_x films with alloying no or little carbon have enough availability of sulphur to form soft WS_2, thus giving rise to a low hardness. Higher carbon content promotes the formation of C-based phases. However above ~ 40 at.% C, the hardness and elastic modulus slightly decrease as the coating at 65 at.% C retreats to 9.96 GPa and 96.58 GPa, respectively. Polcar et al. [20] attributed the further hardness reduction to the fact that no more W is available to form W-C bonds because thereafter the dominance of carbon phases takes over considering the only 7 GPa hardness for pure carbon coatings. The hardness of W-S films alloyed with C or deposited under low pressure shows important improvements reaching values one order of magnitude higher than pure WS_x. This behavior suggests changes in the pure WS_x. This behavior suggests changes in the microstructure, where existing pores in the columnar morphology are favorably eliminated and the compactness and density of the films are thus enhanced as reflected in **Figure** 3.3e in comparison to **Figure** 3.2b.

The influence of Ar depositing pressure, and of the carbon content on the tribological properties of WS_2/a-C films under dry or ambient air were investigated in a systematical way by using a pin-on-disk tribometer. As clearly shown in **Figure** 3.7a, for all tribotests below < 5% R_H, the coefficients of friction can stabilize in the ultralow range of 0.017-0.028, almost independently of Ar flow rate and carbon changes. Such a low friction is rarely reported to achieve with un-hydrogenated DLC in dry atmosphere, which usually has a friction coefficient of above 0.1 before graphitization and failure occurs [5]. Therefore the observed low friction is predominantly attributed to the WS_2 lubrication. Low friction of WS_2 is due to the weaker Van der Waals bonds between hexagonal basal planes, offering an easy slip during frictional contact. These slip mechanisms require released WS_2 crystals with basal planes parallel to the sliding direction. As XRD (see **Figure** 3.4b) confirms the presence of hexagonal basal (002) peaks in the low carbon WS_2/a-C coatings, there are reasons to believe that agglomeration of WS_2 nano-grains on the wear tracks are easily formed [39]. In terms of sliding in a humid environment, the CoF evidently increases due to the reactions of WS_2 with water molecules to form inferior lubricant WO_3. The coating at ~ 40 at.% deposited at 10 sccm has the lowest CoF of 0.102. 20 sccm Ar produces a maximum of 0.174, which belongs to the typical CoFs of WS_2 in moist air that are commonly reported to be 0.15-0.20 in Ref. [10, 40].

However, the wear rate of coating is strongly affected by the deposition pressure, carbon content and environmental conditions. With the carbon content at the level of ~ 20 at.%, the wear rate in dry sliding is lower than that in humid tests (see **Figure** 3.7b). For instance, the lowest W_R of 1.84×10^{-7} $mm^3 N^{-1}m^{-1}$ is recorded under 10 sccm Ar in dry air. The W_R goes up with higher Ar flow rates up to 4.11×10^{-7} $mm^3 N^{-1}m^{-1}$

under 25 sccm Ar. Meanwhile, W_R is much higher in humid air (55% R_H), with 2.93×10^{-7} mm^3 $N^{-1}m^{-1}$ deposited under low Ar pressure and 4.37×10^{-7} mm^3 $N^{-1}m^{-1}$ deposited under high Ar pressure, respectively. It could be concluded that higher Ar pressure triggers worse wear resistance, mainly due to a lower hardness and porous structure of the coating. Therefore the coating deposited under 10 sccm Ar is advisable from the anti-wear point of view since no marked CoF reduction is observed in coatings with higher sulphur stoichiometry and crystallinity, as a result of higher Ar flow rate.

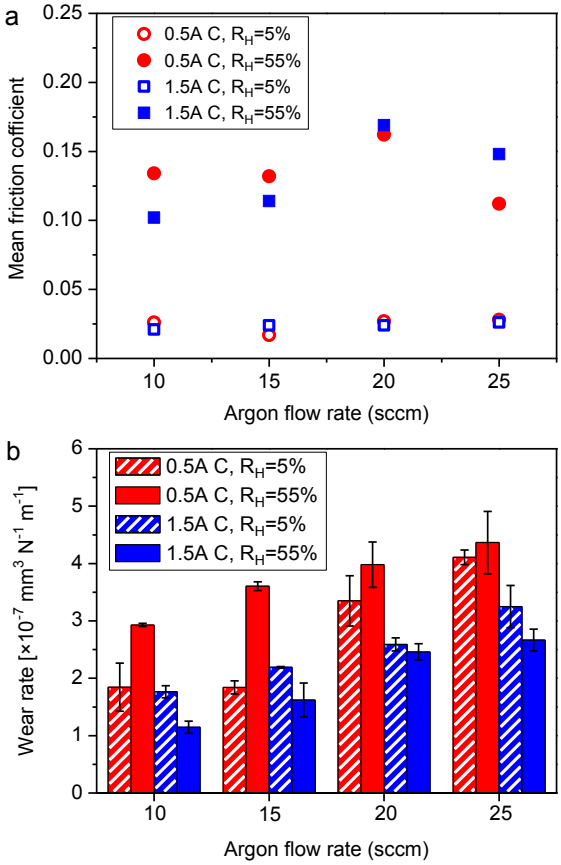

***Figure** 3.7 Tribological performance of WS_2/a-C films as a function of Ar flow rate and carbon content after sliding 1000 m: (a) mean friction coefficient; (b) wear rate.*

In fact, Aubert et al. [41] also pointed out that the sub-stoichiometric MoS_x ($x \approx 1.5$) yields the lowest CoF even compared with the stoichiometric one. The rather low wear rate of low-carbon WS_2/a-C coatings in dry air is primarily attributed to the superior basal WS_2 induced lubrication, i.e. weaker contribution comes from amorphous DLC in the coatings. The addition of C to the level of ~ 40 at.% decreases the W_R for all the ranges of investigated Ar flow rates. Particularly when testing in humid air, W_R seems

to be slightly lower than that tested in dry conditions. This is because carbon additions increase coating density and hardness. Also, DLC initiates to play a predominant role in reducing wear as unhydrogenated DLC generally performs better in moisture.

Further tribological behavior as a function of carbon content (10 sccm Ar) is depicted in **Figure** 3.8. **Figure** 3.8a indicates that under 5% R_H the addition of C up to 40 at.% C reduces the average CoF from 0.039 in pure WS_2 and 0.026 in the ~ 20 at.% C to 0. 021 in the ~ 40 at.% C coating. However, with further carbon additions up to above 51 at.% C, CoFs start to increase to 0.069 for the ~ 65 at.% C coating. Also this changing trend of CoFs with carbon variations is verified at humid testing (see **Figure** 3.8a).

Figure 3.8b shows that W_R decreases with an increasing carbon content until ~ 40 at.% C. Unlike most reported wear life of pure TMD films, which usually exhibit rapid failures [36, 42], **Figure** 8b and c still prove that WS_2 films (~ 3 GPa hardness) deposited in a low pressure could have a low W_R of 4.09×10^{-7} mm^3 $N^{-1}m^{-1}$ after sliding 1000m in dry air. However, the W_R in humid air comes to one magnitude higher, i.e. 5.91×10^{-6} mm^3 $N^{-1}m^{-1}$, indicating the poor wear resistance of WS_2 in moisture.

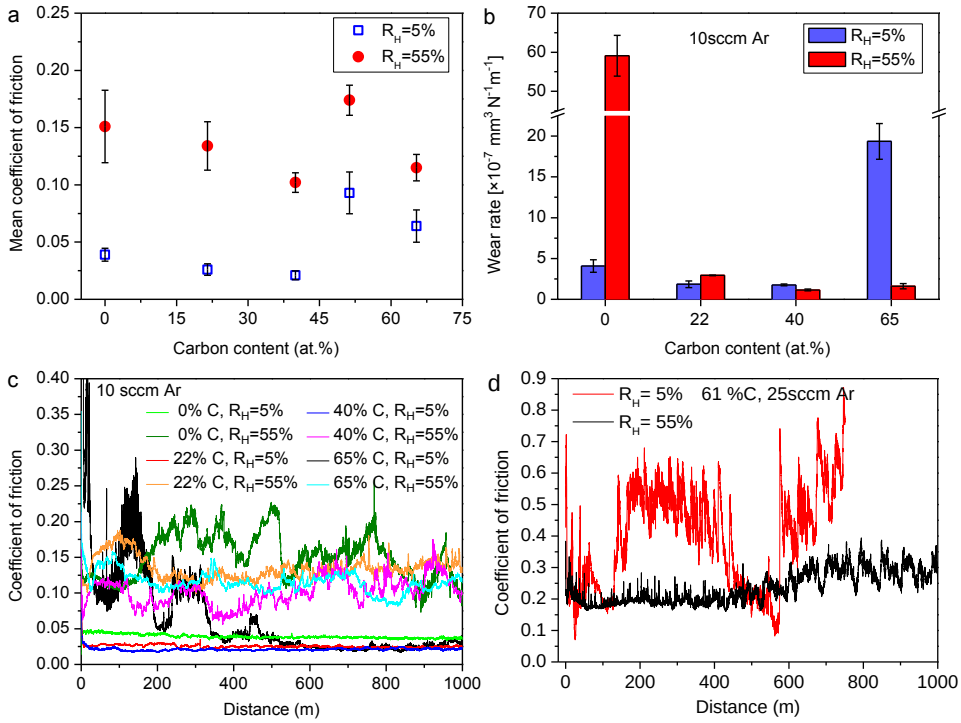

***Figure** 3.8 Tribological performance as a function of carbon content: (a) average coefficient of friction; (b) wear rate; (c) coefficient of friction curves of WS_2/a-C coatings; (d) coefficient of friction curves showing WS_2/a-C with high carbon content deposited under 25 sccm Ar fails in dry sliding.*

Figure 3.9 reveals the confocal 3D topography on wear tracks of sputtered films as a function of carbon content. A relatively narrow wear track (173.80 μm width × 0.84 μm depth) of WS_2 film tested under 5% R_H (**Figure** 3.9a) was formed in contrast to an extraordinary large (407.44 μm width × 1.41 μm depth) track tested under 55% R_H (**Figure** 3.9b). **Figure** 3.9c presents the much reduced depth (0.35 μm) and width (140.15 μm) for the ~ 40 at.% C coating, corresponding to a remarkably low wear rate of 1.76 $\times 10^{-7}$ mm^3 $N^{-1}m^{-1}$ in dry sliding. As pointed out in [2], a W_R of 1 × 10^{-7} mm^3 $N^{-1}m^{-1}$ represents an average removal rate of $<$ 1 atomic layer per cm pass of a counterpart with a standard 5 N load. Therefore, such a low wear and friction coefficient (0.021) potentially fulfill the criteria of self-lubricated wear resistant coatings for aerospace applications, which is proposed to be $< 10^{-6}$ mm^3 $N^{-1}m^{-1}$ for wear rates and $<$ 0.1 for friction coefficients [4].

Although extremely broad diffraction peaks shown in **Figure** 3.4c and disordered phases in **Figure** 3.5f reveal no strong (002) basal planes, extensive research have documented friction induced degree of crystallinity from otherwise amorphous films and realignment of TMD (002) basal planes. In other words, the WS_2/a-C film can adapt itself during contact forcing the small crystallites to favor an orientation where their basal planes are parallel to the mechanical contact, and thereby attaining ultralow friction values [2, 39, 43, 44]. **Figure** 3.10 shows the Raman spectra on wear tracks under different conditions. **Figure** 3.10a indicates the sputtered a-C coating is Raman active in the 1300–1600 cm^{-1} region, corresponding to the typical D (1380 cm^{-1}) and G (1550 cm^{-1}) peaks of amorphous carbon and also E^1_{2g} (355 cm^{-1}) and A^1_g (421 cm^{-1}) peaks presenting hexagonal WS_2 [36]. As shown in **Figure** 3.10b, reorientation and conglomeration of oriented hexagonal WS_2 nanograins together DLC peaks are verified on all tracks of dry air sliding. Furthermore, it is clear that the WS_2 phase is rich in low-carbon coatings while in high-carbon WS_2/a-C the DLC peaks are intensified. The formation of amorphous carbon in wear tracks is detected and is responsible for low friction in moist air, explaining CoF to be around 0.15 approaching the typical friction of DLC in humid conditions. In addition, WO_3 peaks around 710 cm^{-1} and 810 cm^{-1} are presumably detected by Raman in low-carbon WS_2/a-C films (**Figure** 3.10c). EDS mappings also verify varied concentrations of oxygen covering the ball scar (not shown), implying the formation of WO_3. Further increase in carbon to 65 at.% leads to poor wear resistance, particularly in dry air as indicated in **Figure** 3.8b and **Figure** 3.9d. In humid air, increased contribution of the C-based phases decreases wear rate significantly, corresponding to lubrication dominated by DLC. DLC predominantly Raman-active in the tracks of high-carbon coating further confirms this hypothesis (see **Figure** 3.10c).

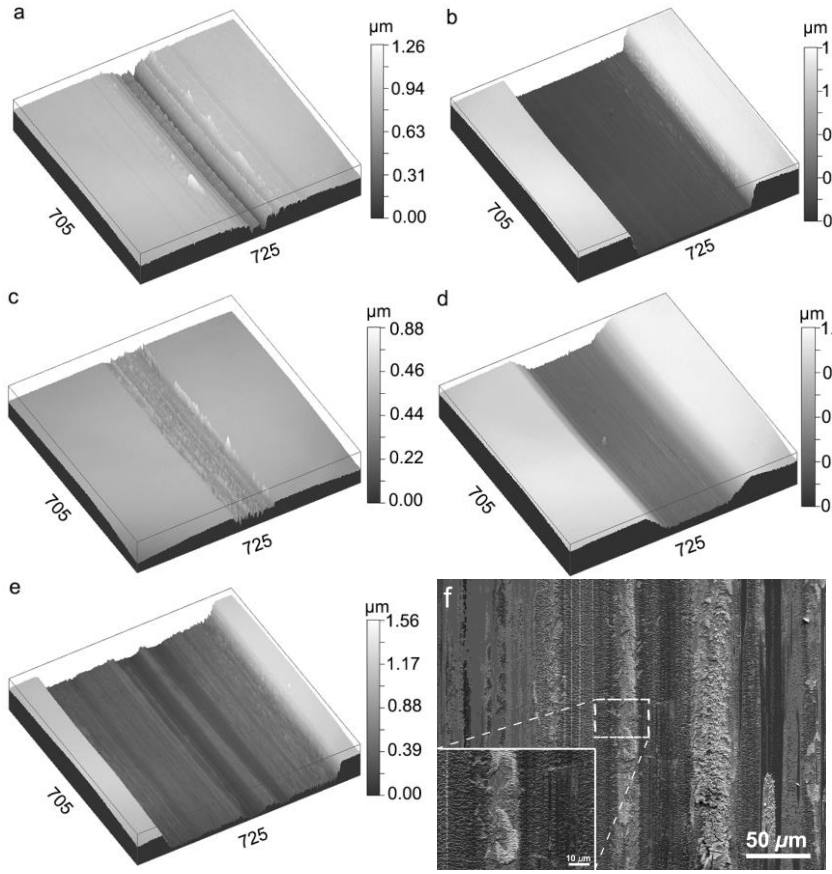

***Figure** 3.9 Confocal micrographs (705×725 μm²) showing 3D views of the wear scars as a function of carbon content: (a) 0 at.% C, 5% R_H; (b) 0 at.% C, 55% R_H; (c) 40 at.% C, 5% R_H; (d) 65 at.% C, 5% R_H; (e) 61 at.% C, 25 sccm Ar, 5% R_H; (f) SEM image confirming fully delaminated coating of (e). Note: besides (e) was tested for 750 m due to earlier failure, all others were sliding for 1000 m.*

In particular the coatings with the same high carbon content but deposited at high pressure exhibit catastrophic failure. In fact, the third-body graphitic debris are quickly formed, leading to an instant high CoF of ~ 0.6 (within only 200 m), a typical value of dry sliding of direct metal contact [45] (see **Figure** 3.8d). Fully delaminated topography is clearly visible in **Figure** 3.9e and confirmed by SEM observations, see **Figure** 3.9f. Similar wear behavior was found in Mo-Se-C system [46], i.e. the highest carbon content (58 and 68 at.%) coatings fail to survive to low R_H. These justify the conclusion that WS_2/a-C coatings with scarce sulphur perform worse in dry conditions, consistent with the findings by Voevodin et al. [5]. Thus, a relatively high absolute content of sulfur in the coatings rather than only high S/W ratio should be taken into consideration.

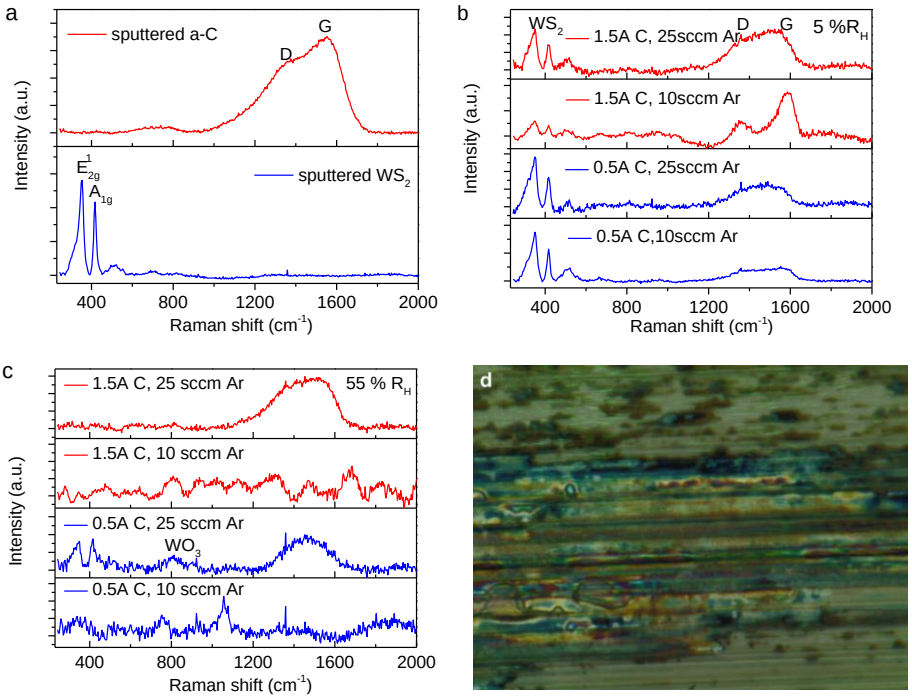

***Figure** 3.10 Raman spectra of the a-C, WS_2 and WS_2/a-C coatings in the wear tracks after sliding 1000 m under different deposition conditions: (a) as-sputtered a-C and WS_2 films; (b) wear tested under 5% R_H; (c) wear tested under 55% R_H; (d) A typical wear morphology of WS_2/a-C coatings (0.5A C, 10 sccm Ar) in dry sliding.*

In addition, from **Figure** 3.8c an interesting observation is that coatings with a carbon content < 40 at.% have rather low initial CoFs in dry air (0.013, 0.127, 0.185 respectively for pure WS_2 films, 20 at.% C, 40 at.% C) and it only takes around 10m to stabilize; thereafter it remains extremely stable (~ 0.02) during the rest testing. In the case of 65 at.% C, a transient CoF of 0.568 is observed and it further increases to ~ 0.8. After fluctuating within about 500 m with a decreasing tendency, it falls to 0.02. This implies CoF reduces with the number of cycles for the high-carbon WS_2/a-C deposited under low pressure. The deficient sulfur (~ 20 at.%) in high-carbon WS_2/a-C entails a longer time to accumulate or align WS_2 crystallites along the sliding surface. This explains the extended running-in time before it ultimately approaches the stabilized ultralow CoF value as that of WS_2 rich films.

3.4 CONCLUSIONS

WS_2/a-C nanocomposite coatings were fabricated by magnetron co-sputtering. This work leads to an in-depth understanding of the synergetic effects of carbon content

and deposition pressure on the S/W stoichiometry, surface morphology, microstructure and related structure-property relationship.

- The coatings consist of approximately 10–40 at.% W, 20–65 at.% C, and 20–60 at.%. S, with neglecting 1–3 at.% oxygen contamination. The S/W stoichiometric ratio is larger in lamellar films and smaller in compact films. Crystallinity is found to be improved by a high Ar pressure, which also elucidates larger lamellae size and roughened surface. Preferential sputtering of sulphur reinforced by impingement at low Ar pressure explains a low stoichiometric ratio in the coatings.
- TEM reveals obvious feathery WS_2 platelets randomly distributed in amorphous carbon matrix, and the nanocomposite coating turns more amorphous-like when carbon content increases. XRD confirms favorable basal plane orientation (002) in WS_2/a-C coatings with increasing carbon concentration up to ~ 22 at.%. Nanoindentation tests show that the hardness and elastic modulus of the coatings increase one magnitude higher as compared with pure WS_2 films via alloying carbon or alternatively decreasing argon flow rate from 25 sccm to 10 sccm.
- CoF as low as 0.02 could be reached in dry air (< 5% R_H) in all investigated compositional variations of coatings below 51 at.% C. Moreover, CoF remains very stable within 1000 m and appears to be almost independent of S/W ratio (x from 1.31 to 1.76). On the other hand, CoF goes up to 0.15 in moisture.
- Pure WS_2 films deposited under a low pressure can survive over 1000m dry sliding. WS_2/a-C coating with ~ 40 at.% C exhibits the best wear resistance while the high-carbon coating (~ 65 at.% C) easily fails in dry air. Although high Ar flow rates could enhance the crystallinity of WS_2 and yield higher S/W ratio, the appropriately lower deposition pressure, promoting hardness and low wear rate, is recommended from a tribological point of view.

REFERENCES

[1] S. Prasad, J. Zabinski, Super slippery solids, *Nature* 387 (**1997**) 761-763.

[2] C. Muratore, A.A. Voevodin, Chameleon Coatings: Adaptive Surfaces to Reduce Friction and Wear in Extreme Environments, *Annu. Rev. Mater. Res.* 39 (**2009**) 297-324.

[3] T. Spalvins, National Aeronautics and Space Administration, Cleveland, OH (USA). Lewis Research Center, **1984**.

[4] A.A. Voevodin, J.S. Zabinski, Nanocomposite and nanostructured tribological materials for space applications, *Compos. Sci. Technol.* 65 (**2005**) 741-748.

[5] A.A. Voevodin, J.P. O'Neill, J.S. Zabinski, Nanocomposite tribological coatings for aerospace applications, *Surf. Coat. Tech*. 116–119 (**1999**) 36-45.

[6] Y.T. Pei, D. Galvan, J.T.M. De Hosson, A. Cavaleiro, Nanostructured TiC/a-C coatings for low friction and wear resistant applications. *Surf. Coat.Tech*. 198 (**2005**) 44-50.

[7] J. Fontaine, C. Donnet, A. Erdemir, Fundamentals of the tribology of DLC coatings, in: C. Donnet, A. Erdemir (Eds.), Tribology of diamond-like carbon films: Fundamentals and applications, Springer US, Boston, MA, **2008**, pp. 139-154.

[8] Y.T. Pei, D. Galvan, J. Th.M. Dehosson, Nanostructure and properties of TiC/a-C:H composite coatings, *Acta Mater*. 53 (**2005)** 4505-4521.

[9] L. Gu, P. Ke, Y. Zou, X. Li, A. Wang, Amorphous self-lubricant MoS_2-C sputtered coating with high hardness, *Appl. Surf. Sci*. 331 (**2015**) 66-71.

[10] A.A. Voevodin, J.S. Zabinski, Supertough wear-resistant coatings with 'chameleon' surface adaptation, *Thin Solid Films* 370 (**2000**) 223-231.

[11] H. Dimigen, H. Hübsch, P. Willich, K. Reichelt, Stoichiometry and friction properties of sputtered MoS_x layers, *Thin Solid Films* 129 (**1985**) 79-91.

[12] A. Nossa, A. Cavaleiro, The influence of the addition of C and N on the wear behaviour of W–S–C/N coatings, *Surf. Coat. Tech*. 142–144 (**2001**) 984-991.

[13] M. Evaristo, T. Polcar, A. Cavaleiro, Tribological behavior of C-alloyed transition metal dichalcogenides (TMD) coatings in different environments, *Int. J. Mech.and Mater. Des*. 4 (**2008**) 137-143.

[14] G. Weise, N. Mattern, H. Hermann, A. Teresiak, I. Bächer, W. Brückner, H.D. Bauer, H. Vinzelberg, G. Reiss, U. Kreissig, M. Mäder, P. Markschläger, Preparation, structure and properties of MoS_x films, *Thin Solid Films* 298 (**1997**) 98-106.

[15] T. Polcar, M. Evaristo, A. Cavaleiro, The tribological behavior of W–S–C films in pin-on-disk testing at elevated temperature, *Vacuum* 81 (**2007**) 1439-1442.

[16] M. Evaristo, T. Polcar, A. Cavaleiro, Synthesis and properties of W–Se–C coatings deposited by PVD in reactive and non-reactive processes, *Vacuum* 83 (**2009**) 1262-1265.

[17] J. Xu, L. Chai, L. Qiao, T. He, P. Wang, Influence of C dopant on the structure, mechanical and tribological properties of r.f.-sputtered MoS_2/a-C composite films, *Appl. Surf. Sci*. 364 (**2016**) 249-256.

[18] M.-j. Dai, C.-b. Wei, K.-s. Zhou, M. Zhu, H.J. Hou, S.S. Lin, X. Tong, Properties of W/DLC/W–S–C composite films fabricated by magnetron sputtering, *Trans. Nonferrous Met. Soc. China* 25 (**2015**) 3002-3011.

[19] J. Sundberg, R. Lindblad, M. Gorgoi, H. Rensmo, U. Jansson, A. Lindblad, Understanding the effects of sputter damage in W–S thin films by HAXPES, *Appl. Surf. Sci.* 305 (**2014**) 203-213.

[20] T. Polcar, A. Nossa, M. Evaristo, A. Cavaleiro, Nanocomposite coatings of carbon-based and transition metal dichalcogenides phases: A review, *Rev. Adv. Mater. Sci.* 15 (**2007**) 118-126.

[21] M. Evaristo, A. Nossa, A. Cavaleiro, W–S–C sputtered films: Influence of the carbon alloying method on the mechanical properties, *Surf. Coat. Tech.* 200 (**2005**) 1076-1079.

[22] F. Lévy, J. Moser, High-resolution cross-sectional studies and properties of molybdenite coatings, *Surf. Coat. Tech.* 68–69 (**1994**) 433-438.

[23] A. Nossa, A. Cavaleiro, N.J.M. Carvalho, B.J. Kooi, J.T.M. De Hosson, On the microstructure of tungsten disulfide films alloyed with carbon and nitrogen, *Thin Solid Films* 484 (**2005**) 389-395.

[24] C.S. Sandu, T. Polcar, A. Cavaleiro, TEM investigation of MoSeC films, *Microsc. Microanal.* 14 S3 (**2008**) 7-10.

[25] H. Dimigen, H. Hubsch, P. Willich, K. Reichelt, Lubrication properties of r.f. sputtered MoS_2 layers with variable stoichiometry, *Thin Solid Films* 64 (**1979**) 221.

[26] E. Särhammar, E. Strandberg, J. Sundberg, H. Nyberg, T. Kubart, S. Jacobson, U. Jansson, T. Nyberg, Mechanisms for compositional variations of coatings sputtered from a WS_2 target, *Surf. Coat. Tech.* 252 (**2014**) 186-190.

[27] M. Regula, C. Ballif, J.H. Moser, F. Lévy, Structural, chemical, and electrical characterization of reactively sputtered WS_x thin films, *Thin Solid Films* 280 (**1996**) 67-75.

[28] M. Ohring, Chapter 5 - Plasma and ion beam processing of thin films, in: Materials science of thin films (2nd ed.), Academic Press, San Diego, **2002**, pp. 203-275.

[29] X. Zhang, L. Qiao, L. Chai, J. Xu, L. Shi, P. Wang, Structural, mechanical and tribological properties of Mo–S–N solid lubricant films, *Surf. Coat. Tech.* 296 (**2016**) 185-191.

[30] D.Y. Wang, C.L. Chang, W.Y. Ho, Microstructure analysis of MoS_2 deposited on diamond-like carbon films for wear improvement, *Surf. Coat. Tech.* 111 (**1999**) 123-127.

[31] J.A. Thornton, Influence of apparatus geometry and deposition conditions on the structure and topography of thick sputtered coatings, *J. Vac. Sci. Technol.* 11 (**1974**) 666-670.

[32] C.R.D. Priestland, S.D. Hersee, The effects of pressure on the deposition rate in rf sputtering processes, *Vacuum* 22 (**1972**) 103-106.

[33] J. Moser, F. Lévy, Growth mechanisms and near-interface structure in relation to orientation of MoS_2 sputtered thin films, *J. Mater. Res.* 7 (**1992**) 734-740.

[34] J. Sundberg, H. Nyberg, E. Särhammar, F. Gustavsson, T. Kubart, T. Nyberg, S. Jacobson, U. Jansson, Influence of Ti addition on the structure and properties of low-friction W–S–C coatings, *Surf. Coat. Tech*. 232 (**2013**) 340-348.

[35] T. Polcar, M. Evaristo, A. Cavaleiro, Comparative study of the tribological behavior of self-lubricating W–S–C and Mo–Se–C sputtered coatings, *Wear* 266 (**2009**) 388-392.

[36] T.W. Scharf, A. Rajendran, R. Banerjee, F. Sequeda, Growth, structure and friction behavior of titanium doped tungsten disulphide (Ti-WS_2) nanocomposite thin films, *Thin Solid Films* 517 (**2009**) 5666-5675.

[37] T. Polcar, M. Evaristo, A. Cavaleiro, Self-Lubricating W–S–C Nanocomposite Coatings, *Plasma Process. Polym*. 6 (**2009**) 417-424.

[38] T. Polcar, M. Evaristo, R. Colaço, C. Silviu Sandu, A. Cavaleiro, Nanoscale triboactivity: The response of Mo–Se–C coatings to sliding, *Acta Mater*. 56 (**2008**) 5101-5111.

[39] T.W. Scharf, S.V. Prasad, Solid lubricants: A review, *J. Mater. Res*. 48 (**2013**) 511-531.

[40] S.V. Prasad, J.S. Zabinski, N.T. McDevitt, Friction behavior of pulsed laser deposited tungsten disulfide films, *Tribol. Trans*. 38 (**1995**) 57-62.

[41] A. Aubert, J.P. Nabot, J. Ernoult, P. Renaux, Preparation and properties of MoSx films grown by d.c. magnetron sputtering, *Surf. Coat.Tech*. 41 (**1990**) 127-134.

[42] N.M. Renevier, J. Hamphire, V.C. Fox, J. Witts, T. Allen, D.G. Teer, Advantages of using self-lubricating, hard, wear-resistant MoS_2-based coatings, *Surf. Coat. Tech*. 142–144 (**2001**) 67-77.

[43] T. Polcar, A. Cavaleiro, Review on self-lubricant transition metal dichalcogenide nanocomposite coatings alloyed with carbon, *Surf. Coat. Tech*. 206 (**2011**) 686-695.

[44] F. Gustavsson, S. Jacobson, A. Cavaleiro, T. Polcar, Ultra-low friction W–S–N solid lubricant coating, *Surf. Coat. Tech*. 232 (**2013**) 541-548.

[45] Y.T. Pei, D. Galvan, J.T.M. De Hosson, Tribological behavior and thermal stability of TiC/a-C:H nanocomposite coatings, *J. Vac. Sci. Technol*. 24 (**2006**) 1448-1453.

[46] T. Polcar, M. Evaristo, M. Stueber, A. Cavaleiro, Mechanical and tribological properties of sputtered Mo–Se–C coatings, *Wear* 266 (**2009**) 393-397.